

LCZ scheme for assessing Urban Heat Island intensity in a complex urban area (Beirut, Lebanon)



Nada Badaro-Saliba^{a,*}, Jocelyne Adjizian-Gerard^a, Rita Zaarour^a, Georges Najjar^b

^a CREEMO Laboratory, Geography Department, Saint-Joseph University, Beirut, Lebanon

^b ICube Laboratory, UMR 7357 CNRS-University of Strasbourg, Illkirch, France

ARTICLE INFO

Keywords:

Urban Heat Island
Remote sensing
Local climate zone
Topography
Random forest
ANOVA
Beirut

ABSTRACT

Thermal remote sensing has become widely used to monitor and study Urban Heat Island (UHI) by the use of satellite Land Surface Temperature (LST) data, and the Local Climate Zone (LCZ) scheme has established itself as the standard for assessing Urban Heat Island Intensity (UHII). A lot of research on LST-LCZ relationship has been done, but mainly in flat terrain. Some studies on UHI in mountainous areas have been conducted, but most of them considered the combined effect of land use/land cover and topography on temperature. To the best of our knowledge no study has been carried out on the LST-LCZ relationship in a complex topography area after removing the topography effect. This paper presents a methodology for assessing the impact of the urban structure on UHII in Beirut, a coastal city with heterogeneous urban morphology and complex topography. It was concluded that the main urban variables which contribute to the spatial variability of topographically normalized LST are, in decreasing order of relative importance, the built-up ratio, the pervious surface ratio, the buildings' mean height and mean surface area. The difference in average temperatures between high-rise densely built LCZs and mostly pervious zones exceeded two degrees at nighttime.

1. Introduction

Urban Heat Island (UHI) designates the fact that an urban area is warmer than its surrounding rural area (Santamouris, 2015). This phenomenon is due to anthropogenic modifications of the surface energy and radiation balance which accompany urban development (Oke, 1988; Arnfield, 2003). This contrast in temperature can be observed either on the surface (Surface Urban Heat Island: SUHI) or in the air (Hu et al., 2019). The term UHI usually refers to air temperature near the ground (Urban Canopy Layer Heat Island: UCL-UHI). This elevation of ambient air temperature can have an adverse effect on health and comfort of human beings (Goggins et al., 2012; Heaviside et al., 2016) and contributes to the increase in energy consumption, leading to an increase in air pollution (US EPA, 2014b). It is therefore important to identify the factors that contribute to the formation of the UHI and link them to the UHI magnitude to take the right mitigation measures. Urban heat island is affected by natural factors (synoptic weather, climate, time of the day, period of the year, topography) and city form and function factors (city size, urban morphology, land cover, anthropogenic heat fluxes) (Oke, 1982). Two cities, with similar urban structure but with different geographic context, may be quite different in term of UHI magnitude. UHI is affected by background climate (Yu et al., 2018; Manoli et al., 2019; Li et al., 2020) and synoptic weather (Hais and Kucera, 2009). It is

* Corresponding author.

E-mail addresses: nada.saliba@usj.edu.lb (N. Badaro-Saliba), jocelyne.gerard@usj.edu.lb (J. Adjizian-Gerard), rita.zaarour@usj.edu.lb (R. Zaarour), georges.najjar@unistra.fr (G. Najjar).

strongest in hot weather (Founda and Santamouris, 2017), dry (Imamura, 1970) clear and calm (US EPA, 2014a). It is affected by time, presenting daily and seasonal variability. It is stronger at night than during the day. During the day, impervious surfaces and buildings heat up and store a lot of energy, while vegetation and pervious surfaces do not warm up much due to evapotranspiration. The solar radiation absorbed by materials during the day is slowly restored in the form of heat during the night. Consequently, at night, the air in non-urbanized areas will cool quickly, while urban areas will limit this cooling (Delami et al., 2018). Seasonal variability is due to variation in incoming solar radiation (Zhou et al., 2016), to modification of the surface cover such as vegetation (Stroppiana et al., 2014) and to modification of prevailing meteorological conditions as well (Manoli et al., 2020). More importantly, local topography may affect greatly UHI, by modifying surface air variables, mainly air temperature (elevation), solar radiation reaching the surface (slope, orientation), wind speed and direction (Ruel et al., 1998; Lookingbill and Urban, 2003; Zhou et al., 2020).

The urban heat island is characterized by its intensity (UHII), which was first expressed as the difference between a background rural reference site and the urban temperatures (Tzavali et al., 2015). But according to Stewart and Oke (2009), this definition raises several problems: it is not always easy to qualify a site as urban or rural as there are no universal definitions for these terms (Stewart and Oke, 2009). The urban/rural classification is too restrictive, it does not take into consideration suburban areas for instance. Furthermore, the urban-rural temperature difference may be misleading in assessing the increase in temperature due to urbanization. Martilli et al. (2020) pointed out very clearly that "UHI magnitude is a function of both urban and rural features. In other words, two cities with very similar structure, materials, cover and population may experience very different UHI magnitudes based solely on the differing characteristics of their rural surroundings" (Martilli et al., 2020). The problem is even more complex in a relief or coastal area, as topography and water bodies play a key role in the spatial variability of air temperature (Bokwa et al., 2015; Gercek et al., 2016). The topography effect may increase, decrease, or mask this excess heat. This could be the case, for instance, when the rural and urban areas are at different altitudes or located on slopes with different orientations. To overcome these problems, Stewart and Oke developed the Local Climate Zone (LCZ) scheme, a climate-based classification of urban and rural areas. They define "local climate zones as regions of uniform surface cover, structure, material, and human activity that span hundreds of meters to several kilometers in horizontal scale. Each LCZ has a characteristic screen-height temperature regime that is most apparent over dry surfaces, on calm, clear nights, and in areas of simple relief." (Stewart and Oke, 2012). Consequently, UHI magnitude is expressed as an LCZ temperature difference rather than an urban-rural difference.

There is more and more interest in intra-urban UHII assessment, again for urban-heat mitigation purpose, as studies have shown that people living in hotter parts of the city are at greater health risk, compared to those living in colder parts, during extreme heat episodes (Smargiassi et al., 2009). The temperature difference between hot and cold parts of a city can reach a few degrees (Yan et al., 2014; da Silva et al., 2018). The LCZ typology has proven to be efficient in identifying intra-urban areas with different thermal behavior, and therefore in capturing the spatial and temporal variability of surface and urban canopy temperature due to urban development (Richard et al., 2018). The LCZ scheme is generic enough to be used in different contexts, facilitating inter-city comparison (Bechtel et al., 2015, 2019; Gholami and Beck, 2019; Hidalgo et al., 2019). As such, it is widely used nowadays for urban climate studies, and was applied to various domains (mapping, monitoring, UHI, modeling, health, energy, pollution...) and to cities located in very different climatic and geographic contexts (Alexander et al., 2015; Alexander et al., 2016; Brousse et al., 2016; Manandhar et al., 2019; Das et al., 2020; Dian et al., 2020; Xue et al., 2020; Yang et al., 2020).

As said previously, UHI is affected by natural and anthropogenic factors. As it is impossible to modify the natural factors, the only mitigation measures that can be taken concern those of urban development and the LCZ scheme is useful for this (Martilli et al., 2020). It gives a framework to assess the effect of urbanization on temperature (Alexander and Mills, 2014; Cai et al., 2017a; Quan, 2019; Lotfian et al., 2019). It is a basis for identifying the relative contribution of surface structure, surface cover, construction materials and anthropogenic heat emissions to intra-urban UHII which are valuable information at the destination of urban planners and decision makers for UHI mitigation (Mughal et al., 2019; Shi et al., 2019). According to Martilli et al. (2020), "it can help determine which configurations should be chosen for future urban developments, and which urban heat mitigation strategies are most suitable for each type of urban zone in a particular geographical and climatic context" (Martilli et al., 2020).

Remotely sensed land surface temperature (LST) has been widely used to monitor and study UHI (Voogt and Oke, 2003; Zhou et al., 2018) due to the availability of continuous thermal remote sensing data at no cost. It is increasingly being used also in spatial epidemiology (Johnson et al., 2011), to quantify human heat exposure and to assess heat-related health risk at the urban scale (Tomlinson et al., 2011; Buscail et al., 2012; Chen et al., 2018). More precisely, a study on "The Impact of Heat Islands on Mortality in Paris during the August 2003 Heat Wave" (Laaidi et al., 2012) concluded that exposure of the elderly population to high nighttime temperature presents much more health risks than exposure to high daytime, and that nighttime LST was a good indicator of health risk.

A lot of research on LST-LCZ relationship in different regions of the world have been done (Gholami and Beck, 2019), but either in flat or relatively simple topography areas (Geletic et al., 2016; Cai et al., 2017a, 2017b; Wang et al., 2018; Zhao, 2018). To the best of our knowledge no study has been conducted on LST-LCZ relationship in cities with complex topography, where LST variability may be significantly impacted by topography at a local scale. The interest of studying the thermal contrasts between LCZ for mitigation purpose, is to understand how 3D urban morphology and its underlying surface cover affect the UHII. It is thus necessary to correct LST to topography-induced spatial variability (the other natural factors, i.e. climatic and synoptic weather conditions being invariant at a given time), that is to derive the LST that would be observed under a flat terrain. Separating the effect of surface properties from the effect of local topography will be achieved through topographic normalization. Another interest of such an approach would be for comparative purposes with other cities, this also being one of the goals of the LCZ scheme. Moreover, for the study of UHII, LCZs are more appropriate to be used in areas of simple relief, with climate zones of a minimum diameter of 400-1000 m depending on surface roughness, building geometry and atmospheric stability conditions (Stewart and Oke, 2012).

The aim of the present study is to assess nocturnal SUHII in Beirut city. Nighttime was chosen since studies have shown that high nighttime temperatures in urban areas can greatly affect health, when the UHI is stronger, depriving city dwellers of the cooling effect that can be found in rural areas (Tan et al., 2009). They concluded that there is an intra-urban variability of mortality rate during periods of extreme heat, this rate being positively correlated with the density of urban structures (Gabriel, 2011). It should be noted that thermal contrast between zones is more pronounced at night than during the day not only at the urban/rural scale, but also at the local scale, i.e. among the LCZs located within the city as well (van Hove et al., 2015; Fenner et al., 2017). The choice of SUHI was motivated by the fact that LSTs are continuously available at no cost, that nighttime LST is very well correlated to night air temperature (US EPA, 2014c; Del Pozo et al., 2020), and can be used to assess nocturnal UCL-UHI.

The anarchic urban development which characterizes Beirut, the Lebanese capital, its high population density, and its Mediterranean climate, are favorable conditions for the occurrence of urban heat island. An assessment of UHII of Beirut was carried out by numerical modeling (Ghadban et al., 2020), the urban parameters of the model being tuned at the city level and not at the fine scale of LCZs. On the other hand, an LCZ level 0 classification was performed for Beirut (Kaloustian and Bechtel, 2016), without studying the LCZ-temperature relationship. This paper investigates the effectiveness of the LCZ approach to assess nocturnal UHII in Beirut, a city with a complex topography and a heterogeneous urban morphology, LCZs not meeting, on average, the criteria of 400-1000 m diameter.

2. Study area

Beirut has an area of 20.8 km². It is a cape located on the eastern coast of the Mediterranean Sea. It is bounded to the north and the west by the sea and to the east by mountains, and is therefore subject to land and sea breezes, as well as mountain and valley breezes. Beirut is characterized by a complex topography, made of two hills (Tallet el Khayat and Achrafieh), each at an elevation of 100 m, separated by a pass (Fig. 1). This pass separates two dales: one facing the south and the other one facing the north leading to the sea (Saliba et al., 2013).

The Lebanese capital has a population of around 361,366 (Central Administration of Statistics - Population, 2021). The city is mostly a built area with very few green spaces which occupy 0.64 km² or 3% of the surface. Its highly saturated urban fabric is characterized overall by a high roughness which results from heterogeneity of the buildings in terms of age, height, size, or architecture. In addition, for more than a decade, the trend of vertical densification of the city appears to be increasing especially along the waterfront and in some peri-central neighborhoods (Adjizian-Gérard et al., 2013; Zaarour et al., 2015; Zaarour and Voiron-Canicio, 2020). It knows homogeneity in road transport emissions and in activities. The road network is narrow (a mean width of 9 m) and

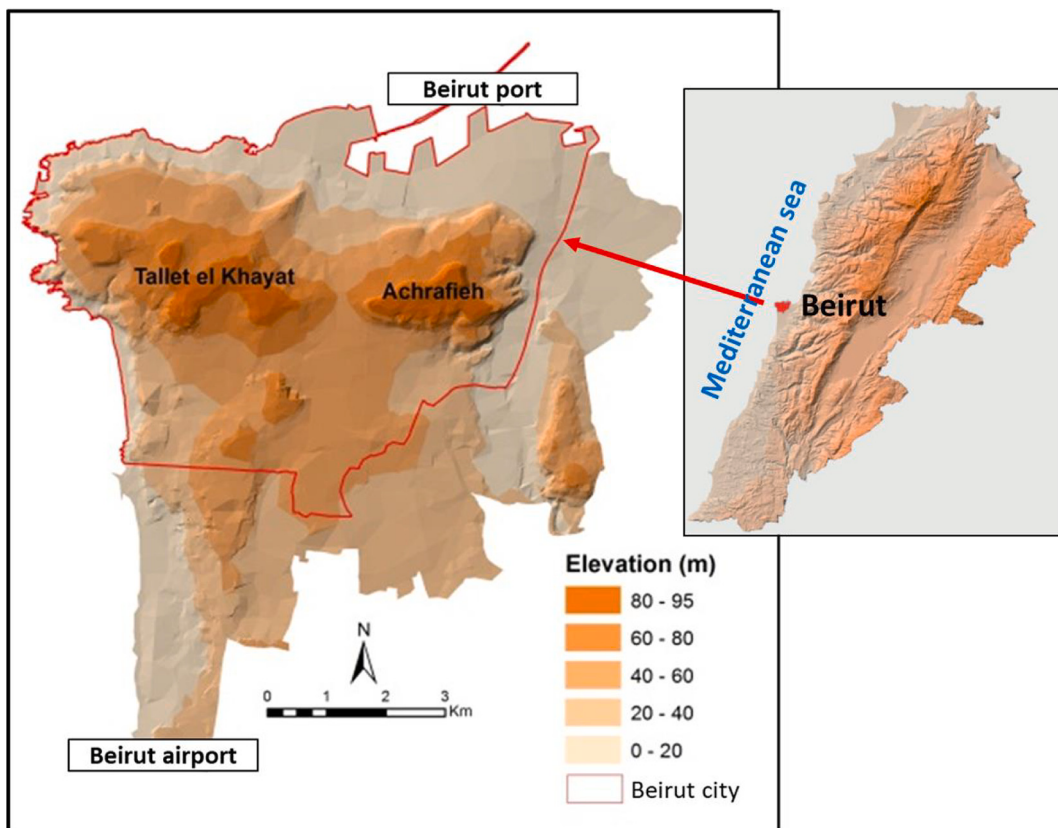
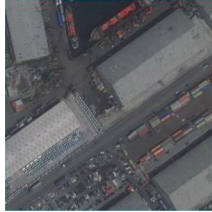


Fig. 1. Topography of Beirut city.

Table 1

Designation of LCZ types (after [Stewart and Oke, 2012](#)). Sample Esri, Maxar images of LCZs in Beirut.

Built types	LCZ 1 compact high-rise	LCZ 2 compact midrise	LCZ 3 compact low-rise	LCZ 4 open high-rise	LCZ 5 open midrise
					
	LCZ 6 open low-rise	LCZ 7 lightweight low-rise	LCZ 8 large low-rise	LCZ 9 sparsely built	LCZ 10 heavy industry
					
Land cover types	LCZ A Dense trees	LCZ B scattered trees	LCZ C bush, scrub	LCZ D low plants	LCZ E bare rock/paved
					
	LCZ F Bare soil/sand	LCZ G Water			
					

dense (325 km of length or 15.6 km/ km²). Finally, Beirut has no significant industries. The port area is located north east.

3. Materials and methods

3.1. LCZ map

An LCZ level 1 classification of Beirut city was produced by the authors for the year 2016, on a 250 m grid. 250 m was found to be the optimal grid size for LCZ mapping in dense urban areas (Lau et al., 2015; Zheng et al., 2018) and was adopted in previous studies on the urban morphology of Beirut (Zaarour et al., 2008; Zarour et al., 2015; Zarour and Voiron-Canicio, 2020). This map was produced using a GIS-based method which is more accurate than the level 0 method, especially in built-up areas (Hidalgo et al., 2019; Xilin et al., 2020). A detailed description of the corresponding methodology will be the subject of a forthcoming research publication (Zaarour et al., 2021). Nevertheless, for the sake of clarity, it is necessary to present an overview of the LCZ classification process. Stewart and Oke have defined seventeen LCZ types (Table 1), characterized by intervals of values associated with geometric and surface cover properties (Table 2).

These parameters were first calculated for each grid cell, using (1) the building footprints with the associated building heights; (2) the road network with the associated road widths; and (3) a Sentinel 2 satellite image. The two GIS vector layers, e.g. the building heights and road network were generated as part of a research on air pollution in Beirut (Chelala et al., 2006, 2007). The building database was updated in 2016, by data from the LIBRIS ANR project (Zaarour et al., 2015), Open Street Map data, digitization from high resolution google earth images and field survey. A cloud free Sentinel 2 image, freely available, dating from July 2016, was downloaded from the United States Geological Survey website (EarthExplorer, 2021). Calculation methods are presented in Table 3. As the cells LCZ types are unknown prior to classification, the AR and HRE parameters were considered as the mean height-to-width ratio of streets and geometric average of building heights respectively. The building heights vector layer was converted to a raster layer, ground pixels being set to zero, to produce a 1 m Digital Object Model (DOM).

Secondly, each cell was assigned to the LCZ to which it is closest regarding the default intervals of values of the seven parameters (Geletič and Lehnert, 2016). Accuracy assessment was based on field work and on a careful visual interpretation of high resolution google earth images on a cell by cell basis. The port area, to the north-east of the city, was assigned to LCZ 10 as to remain in line with what has been done in other cities such as Barcelona, Dublin, Huston... as visualized through the Geopedia online mapping tool (Geopedia - Wudapt, 2021). Moreover, it is the only area classified as such since there is no industry in Beirut city.

Thirteen LCZ classes (Fig. 2), out of the seventeen standard classes of the LCZ scheme are represented in Beirut, nine in the built types and four in the natural land cover types.

3.2. Satellite data

Two types of satellite data, Land Surface Temperature and Digital Elevation Model (DEM) from Advanced Spaceborne Thermal Emission and Reflection Radiometer (ASTER), were used. Both products are freely available from the Land Processes Distributed Active Archive Center (LPDAAC) through the NASA Earthdata Search web application.

ASTER Surface Kinetic Temperature (AST_08) is generated using five Thermal Infrared (TIR) bands (acquired either at daytime or at nighttime) between 8 and 12 μm spectral range. It contains surface temperatures at 90 m spatial resolution for the land areas only (Spacesystems, 2001). Its relative accuracy is equal to 0.3 degrees (ASTER User Handbook, 2021).

Three nighttime images, with dates close to that of the LCZ map, under clear and calm weather conditions, favorable to the development of UHI, spanning over Beirut, available on demand, were ordered and downloaded from the LPDACC website (AST_08.003, 2001): the first date is in spring, during a warm and dry period (June 7, 2016), and the two others in autumn, following a wet period, one during a warm day (October 11, 2015) and the other during a cold day (December 7, 2015). ASTER data is provided in HDF-EOS format, with geographic dimensions of 60 km * 60 km. The three images have been sub-set to the study area, re-projected to the Universal Transverse Mercator projection, Zone 36 N, and exported to Geotiff with the NASA's HDF-EOS To GeoTIFF Conversion Tool (HEG-C, 2017).

The downloaded ASTER Global Digital Elevation Model is produced at 30 m spatial resolution and provided in Geotiff format (ASTER GDEM, 2001).

Table 2

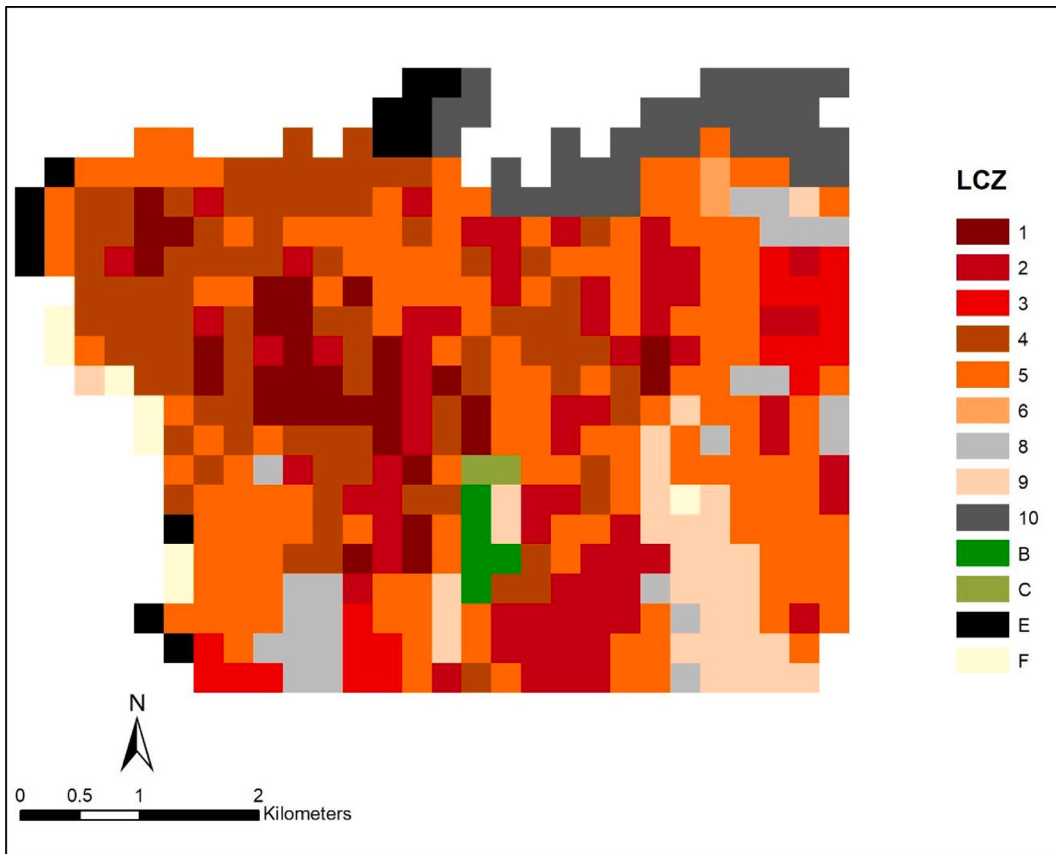
Definition of geometric and surface properties of LCZ types (Stewart and Oke, 2012).

Parameter	Property	Definition
SVF	Sky view factor	Ratio of the amount of sky hemisphere visible from ground level to that of an unobstructed hemisphere
AR	Aspect ratio	Mean height-to-width ratio of street canyons (LCZs 1–7), building spacing (LCZs 8–10), and tree spacing (LCZs A–G)
BSF	Building surface fraction	Ratio of building plan area to total plan area
ISF	Impervious surface fraction	Ratio of impervious plan area (paved, rock) to total plan area
PSF	Pervious surface fraction	Ratio of pervious plan area (bare soil, vegetation, water) to total plan area
HRE	Height of roughness elements	Geometric average of building heights (LCZs 1–10) and tree/plant heights (LCZs A–F) (m)
TRC	Terrain roughness class	Davenport et al.'s (2000) classification of effective terrain roughness (z_0) for city and country landscapes

Table 3

Calculation methods of geometric and surface properties of LCZ types.

Parameter	Raw data (year 2016)	Calculation method	References/Comments
SVF	DOM	SAGA-GIS to calculate 1 m SVF (both ground and roof top pixels) Average ground pixels SVF values	(Bernard et al., 2018)
HRE	Building heights footprints	$\frac{\sum_{i=1}^N (BS_i * BH_i)}{\sum_{i=1}^N BS_i}$ BS_i is the area of building i BH_i is the height of building i N is the number of buildings	(Xu et al., 2017)
SW	Road network	$\frac{\sum_{i=1}^N (RL_i * RW_i)}{\sum_{i=1}^N RL_i}$ RL_i is the length of road i RW_i is the width of road i N is the number of roads	SW is the geometric average of road widths
AR	HRE, SW	$\frac{HRE}{SW}$	(Wicki and Parlow, 2017; Zheng et al., 2018)
BSF	Building footprints	$\frac{\sum_{i=1}^N BS_i}{CS}$ BS_i is the area of building i N is the number of buildings CS is the grid cell area	(Xu et al., 2017)
PSF	Sentinel 2 satellite imagery	$\frac{PS}{CS}$ PS is the total area of pervious surface (retrieved by thresholding 10 m NDVI) CS is the grid cell area	$NDVI = \frac{NIR - R}{NIR + R}$
ISF	BSF, PSF	$1 - (BSF + PSF)$	$BSF + PSF + ISF = 1$
TRC	DOM	Urban Multi-scale Environmental Predictor (UMEP) QGIS plug-in to calculate the roughness length z_0 (m) Classify z_0 according to Davenport classification	(Davenport et al., 2000; Lindberg et al., 2018)

**Fig. 2.** LCZ level 1 map of Beirut, year 2016.

3.3. Topographic normalization of LST

Malbeteau et al. (2017) proposed a physical model for topographic normalization (Malbeteau et al., 2017). Physical models may be hard to implement given the difficulty in obtaining the values of some parameters and they are computer intensive. Instead, a statistical model, and more specifically Random Forest regression as proposed by Zhao et al. (2019) was applied (Zhao et al., 2019). Random

Forest algorithm has been widely used for LST downscaling and has proven to give good results in estimating the non-linear relationship between LST, topography variables and surface parameters (Hutengs and Vohland, 2016; Pang et al., 2017; Bartkowiak et al., 2019).

Random Forest (RF) is a machine learning method (Breiman, 2001) used for the prediction of either a categorical variable (classification) or a continuous variable (regression). It is a two-step process: a learning phase to infer the model, a model being a mathematical formulation of a real-world process, by providing training dataset to a machine learning algorithm to learn from. A training dataset is constituted of a dependent variable, the target, and a set of explanatory variables, the predictors. The learning algorithm finds patterns in the training data such that the input predictors correspond to the target. The generated model is used in a second step to make predictions of unknown values in a prediction dataset that has the same associated explanatory variables (Doan and Kalita, 2015). The RF model is a collection of decision trees, it is what is commonly called a forest. Each tree is made up of a subset of the training dataset, for a subset of predictors. These subsets are randomly formed, hence the term Random Forest (Cutler et al., 2012). In case of classification, the predicted value is the mode of the predictions from all trees. In case of regression, the predicted value is the mean value of the predictions from all trees. Main advantages of RF models are the use of numerical values and categorical values as well, the evaluation of the prediction precision, the robustness in the presence of outliers, noise, and overfitting (Hastie et al., 2009). Moreover, apart from predicting, the RF regression model makes it possible to quantify the contribution of each predictor to the total spatial variability of the target and assigns a variable importance score to each predictor (Genauer et al., 2010; Lagomarsino et al., 2017).

The training is used to evaluate the performance of different models, while trying different combination of explanatory variables and tool settings, until reaching a stable and accurate model. A stable model is a model whose variable importance scores are stable over several runs. Model performance is assessed by external way (R-Squared coefficient resulting from the comparison of the predicted values of a validation dataset excluded from model training, to the corresponding observed values) and by internal way as well, by means of the so called out-of-bag error (OOBE). OOBE is the average error for each sample S_i calculated using predictions from the trees that do not contain S_i in their respective bootstrap sample.

As the relationship between LST, topography and urban structure varies over time, the three LST maps were introduced in three separate RF models and a different RF model was created for each date. Introducing them into the same spatio-temporal model would have led to too much complexity.

The first step of the RF process is to identify the potential explanatory variables. The target to be modeled, i.e. nighttime LST, is influenced by local topography (Hais and Kucera, 2009), urban morphology and land cover factors (Tzavali et al., 2015). The most significant topographic factors have been found to be elevation (relative to air temperature), slope and aspect (relative to solar illumination) (Pierce et al., 2005; McCune, 2007; He et al., 2018), and distance to sea from the north and west side (relative to sea-land breeze) (Zhou et al., 2020). Concerning urban morphology and land cover factors, Stewart and Oke (2012) have defined Urban Canopy Parameters (UCP), characterizing the surface structure and surface cover (Table 2), which they identified as those which largely contribute to thermal contrasts at the urban scale during calm, clear evenings (Bechtel et al., 2016). As the urban database used for the LCZ classification of Beirut was available, these parameters were selected as potential explanatory variables. The ISF parameter has been omitted because it is dependent on BSF and PSF (Table 3). On the other hand, another factor has been added, the mean building area, which is an implicit parameter of the LCZ classification, which distinguishes large buildings from small or medium-sized buildings (Table 1).

A given landscape property (the target) can be controlled by explanatory variables at different scales (Florinsky and Kuryakova, 2000; Catani et al., 2013). "Temperature values can be affected by advection effects from the wider surroundings of a particular location" (van Hove et al., 2015). It was important to determine the optimal spatial scales of predictors (Bechtel et al., 2012; Verdonck et al., 2017; Wicki et al., 2018). All the predictors were thus calculated at five different scales (90 m, 150 m, 250 m, 300 m, 350 m) to obtain Scale-Dependent Predictors (SDP). Elevation, slope, and orientation SDPs (SDP_topo) were derived from DEM. First, the 30 m base DEM was resampled at lower resolutions ($DEM_{low} = 90 \text{ m}, 150 \text{ m}, 250 \text{ m}, 300 \text{ m}, 350 \text{ m}$). From this point, there are two main variants to estimate the SDP_topo for each target point (Florinsky and Kuryakova, 2000): (1) derivation of SDP_topo from DEM_{low} followed by interpolation to target points; or (2) interpolation of DEM_{low} to target points, obtaining true-scale DEMs, followed by derivation of SDP_topo from true-scale DEMs. We chose the second option which is easiest to implement because interpolating aspect data requires vector calculation (Grohmann, 2015). The two remaining topographic predictors, i.e. distance to sea from the north and west coastline are scale-independent. Urban Canopy Parameters SDPs were calculated for 90 m, 150 m, 250 m, 300 m and 350 m squared buffers around each LST target point (Gray et al., 2010). They were calculated from the urban database used to elaborate the LCZ map of Beirut according to calculation methods described in Table 3.

The target variable and SDPs were input to train the model. The first task was to select the set of SDPs which best explain the LST spatial variability. It consisted in a three steps process, inspired by what has been done in previous works (Genauer et al., 2010; Gray et al., 2010; Bradter et al., 2013): (1) select the scale-specific predictors (SSP) which correspond to the best scale of each of the potential explanatory variables. It consisted in univariate regression of LST with each factor at each scale and selecting the scale with the best correlation coefficient; (2) build a forest with all the SSPs on 90% of the data set, the remaining 10% were used for validation purpose. Tune the number of trees parameter to ensure a stable model. The other parameters are kept to default value as they perform well on most data sets (Fox et al., 2017). Compute SSPs variable importance (VI) scores; (3) build forests by a stepwise introduction of SSPs according to the descending order of VI scores. A variable is added only if the OOBE decreases. Build a final forest with the selected SSPs from which no points were removed this time. This approach has the advantage of being easy to implement and allows to reduce the number of predictors while ensuring a small OOBE.

The resulting model was reused to predict topographic normalized LST (LST_n) values at the same location than the training dataset,

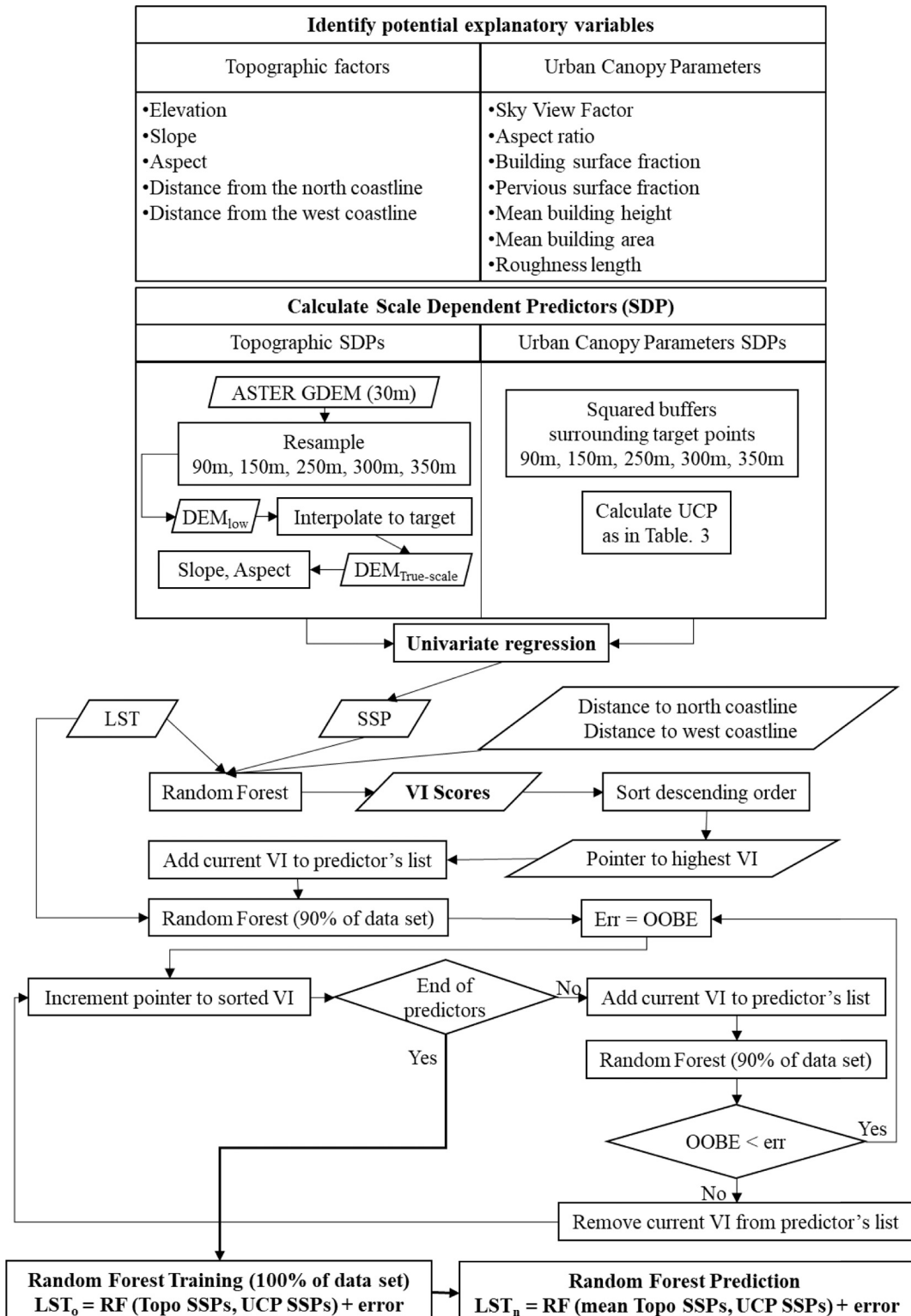


Fig. 3. Flowchart of topographic normalization of LST using Random Forest regression.

with the value for topographic predictors adjusted to a flat terrain (constant values), and unchanged surface variables. After the Random Forest prediction phase, a residual correction was applied to compensate the part of LST variability, which is not explained by the chosen predictors. This consists in adding to the predicted LST_n the difference between the original LST and the LST estimated with the model developed in the training phase (Zhao et al., 2019). This residual correction greatly improved the prediction precision in the case of LST downscaling.

Topographic normalization was accomplished with the Random Forest classification and regression tool of ArcGIS pro, and the whole procedure is depicted in Fig. 3.

Since it is impossible to compare the result of topographic normalization to actual values, the only way to validate the model is by comparing LST maps before and after normalization by exploratory data analysis and visual interpretation.

3.4. UHII assessment

An analysis of variance (ANOVA) approach was performed to uncover significant LST differences between LCZs. A one-way ANOVA omnibus test was first conducted to determine whether any of the mean LST of the different LCZ groups were statistically significantly different from each other. If the omnibus test is significant ($p < 0.001$), it indicates that a difference does exist between the groups but, does not indicate between which groups specifically. In such a case, a Post-Hoc test is performed in order to determine the groups between which mean LST is significantly different (Geletič et al., 2016; Zhao, 2018).

The LCZ map has been superimposed on the topographically normalized LST in a Geographic Information System (ArcGIS). The temperature values corresponding to each LCZ were extracted and exported in a table which was used as input to the one-way ANOVA omnibus and post-hoc tests. Levene's test for homogeneity of variances was performed on the data to check whether the variances of

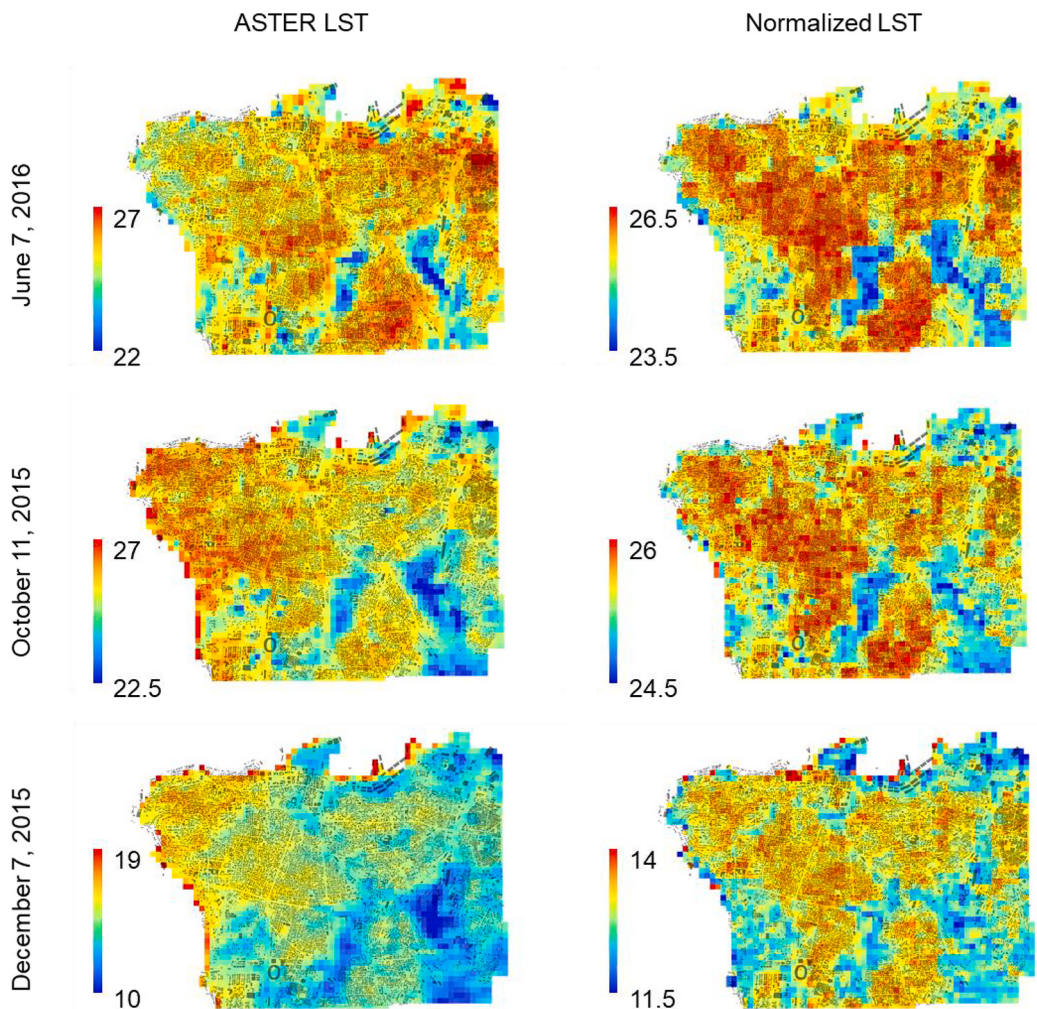


Fig. 4. Images of the LST observed before (left) and after (right) correction for topographic effects on the three ASTER images (June 7, 2016; October 11, 2015 and December 7, 2015). Gray polygons represent buildings.

the different groups were the same. This test failed, indicating that they have unequal variances. Thus, Welch's ANOVA omnibus test was carried out, followed by the Games-Howell Post-Hoc test instead of the classic F-ANOVA omnibus test, followed by TukeyHDS Post-Hoc test. A strict requirement for the classic one-way ANOVA is the equality of variance, while Welch's-ANOVA/Games-Howell is an alternative to the classic F-ANOVA/TukeyHDS which can be used when the data violate the assumption of homogeneity of variances.

After analyzing Post-Hoc Games-Howell results, zones whose LSTs were statistically not significantly different at $p < 0.05$ were grouped, and groups whose mean LST difference were less than the relative accuracy of LST ASTER data were merged. Afterwards, UHII was expressed as the difference in mean LST between group pairs.

Results and discussion

3.5. Topographically normalized map

The best results were obtained with (1) the following topographic predictors: distance from the north coastline, distance from the west coastline, elevation, slope and aspect derived from the 300 m true-scale DEM; (2) and the following UCPs calculated for a 250 m square buffer around the target LST points: building density (ratio of building plan area to total plan area), mean building height, ratio of pervious plan area (bare soil, vegetation, water) to total plan area and mean building area. This spatial resolution has proven to be relevant in other cities as well. (Bechtel et al., 2012; Wicki et al., 2018).

3.6. Model performance and validation

The model performed well for the three dates: on average, OOB and R-Squared coefficient of validation dataset, were 0.15 and 0.8 respectively. Around 80% of LST variation was explained by the model. Comparison of LST maps before and after normalization for the three dates (Fig. 4), clearly shows the removal of the effect of topography on the spatial distribution of the ASTER LST. In a complex environment like Beirut, local topography modifies the surface air variables (air temperature, solar radiation, wind speed and direction) at a pixel-scale, and this topography-induced atmospheric forcing variability may affect greatly the spatial structure of LST (Malbeteau et al., 2017). As this effect varies over time with changes in solar declination (Pierce et al., 2005), the spatial structure of LST due to topography effect will vary as well. On the other hand, in a flat terrain, the spatial variability of urban LST is a result of the composition and structure of the urban surface. The magnitude of this spatial variability is affected by heterogeneity of synoptic weather and by seasonal changes in land cover and soil moisture throughout the year, but its pattern remains unchanged. This was observed for the three dates, as the spatial structure of ASTER LST before normalization is different for the three dates, while the spatial structure of the normalized LST is the same for the three dates, with more or less intensity, and seems to match the spatial distribution of the LCZ map. This indicates that it is worth investigating the normalized LST – LCZ relationship.

A quick look at the box plots (Fig. 5) of LST data before and after removing the effect of topography enables us to detect changes in LST distribution between these different datasets. It is observed that (1) topographic normalization reduces the variability of LST, where range, variance and interquartile range (IQR) of normalized data are lower than initial values for the three dates, with a very significant decrease for the days of October and December (Table 4); (2) the variability of ASTER LST is greater in December than in October and June (which have similar variability), in opposite to normalized LST, where December and October show similar variability which is lower than June. This relative drop is explained by the importance value of topographic vs urban predictors in the RF

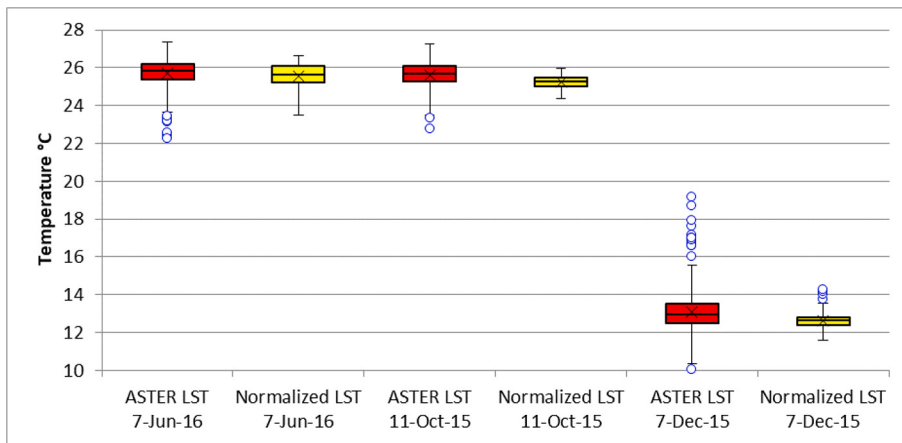


Fig. 5. Box-and-whisker plots of LSTs for the entire study area before (red) and after (yellow) correction for topographic effects on the three ASTER images (June 7, 2016; October 11, 2015 and December 7, 2015). The black cross indicates mean. The line separating box indicates median. The bottom of the box is the first quartile (Q1), and the top is the third quartile (Q3). The lines extending from the boxes (whiskers) represent the highest and the lowest values within 1.5 IQR ($IQR = Q3 - Q1$) from Q3 and Q1. The blue dots are outliers. (For interpretation of the references to colour in this figure legend, the reader is referred to the web version of this article.)

Table 4

Spread of data before (red) and after (yellow) correction for topographic effects on June 7, 2016; October 11, 2015 and December 7, 2015.

	ASTER LST 7-Jun-16	Normalized LST 7-Jun-16	ASTER LST 11-Oct-15	Normalized LST 11-Oct-15	ASTER LST 7-Dec-15	Normalized LST 7-Dec-15
Range without outliers	3.72	3.14	3.78	1.60	5.19	1.99
Standard Deviation	0.73	0.65	0.71	0.30	1.13	0.27
Sample Variance	0.54	0.43	0.50	0.09	1.28	0.07
Range with outliers	5.14	3.14	4.47	1.60	9.34	2.71
IQR	0.84	0.79	0.84	0.44	1.05	0.39

regression model. Relative importance of topography predictors, as calculated by the RF model, increases from June to October to December (55%, 63% and 75% respectively) at the expense of urban canopy predictors (45%, 37% and 25%). This is in line with the fact that when UHII increases, i.e. in hot and dry weather, UHI effect is more related to urban landscape.

Both visual interpretation and exploratory data analysis show that topography effect on temperature has been well removed, isolating the effect of urbanization.

3.7. Welch's ANOVA omnibus test and Games-Howell Post Hoc test

3.7.1. Variations of normalized LST per LCZ

There is a net decrease in the overall variability of normalized LST between June and October/December, as IQR decreased by half (**Table 4**). This download trend between June 7, October 11 and December 7 is also found at the LCZ level (**Fig. 6**): (1) the intra-LCZ variability decreases (indicating that the intra-LCZ heterogeneity of surface properties is well captured in June); (2) the inter-LCZ thermal contrast are less and less intense; (3) the difference in average temperatures between LCZs evolves in the same way, for the three days, but with decreasing intensity; and (4) LSTs of LCZs with abundance of pervious land cover (LCZ 6, 9, B, C and F) in June 7 are lower than those of October 11, while they are higher in the other classes (**Fig. 7**). All this could be explained by (1) the progressive decrease in daily irradiation, UHII is positively correlated with daily irradiation ([He et al., 2018](#)); (2) the loss of vegetation cover and therefore of its cooling power, it was found that vegetation fraction is negatively correlated with LST ([Weng et al., 2004](#)); (3) the increase in pervious soil moisture with reduced soil albedo (greater daytime heat storage) and higher thermal time constant (slow nocturnal cooling) resulting in pervious wet soil warmer than pervious dry soil at night, producing a weaker UHII with moist soil than with dry soil ([Imamura, 1970](#); [Geiger et al., 2003](#)); and (4) a colder weather for the day of December 7, UHII is usually stronger during warm periods ([Tzavali et al., 2015](#)). These findings are in-line with other studies ([Fenner et al., 2017](#); [Hu et al., 2019](#)).

3.7.2. Importance of urban predictors

Welch's ANOVA indicated significant variation among LSTs of the different LCZs for the different dates (p -value <0.001). The grouping of LCZ classes after Post-Hoc Games-Howell ended up with five groups on June 7, three groups on October 11, and two groups on December 7 (**Table 5**). The decreasing number of groups from June to October and December goes hand in hand with the decrease in UHII. The combination of urban predictors (**Table 5**) conditions the temperature of each LCZ. All these UCPs don't have the same importance, and this importance value changes with season and weather type (**Fig. 8**).

In June, building density has the strongest impact on temperature, followed by percentage of pervious land cover. Then, comes with

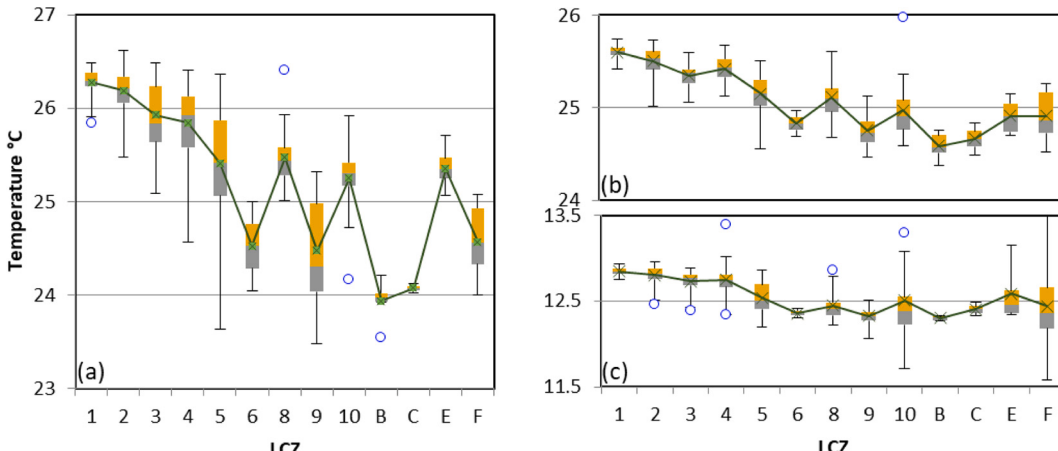


Fig. 6. Box plots of normalized LST per LCZ: June 7, 2016 (a), October 11, 2015 (b), December 7, 2015 (c).

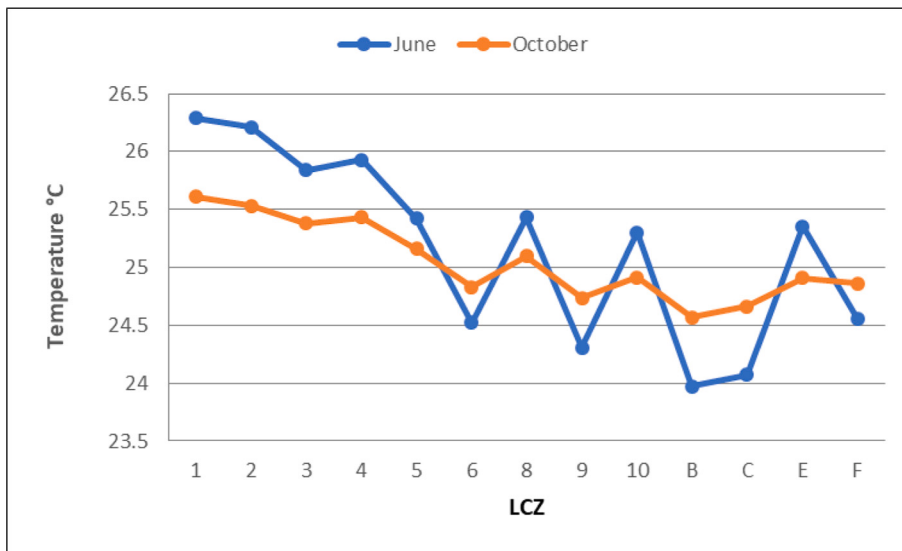


Fig. 7. Average normalized LST as a function of LCZ for June 7, 2016 and October 11, 2015

less importance the impact of building height and average building area. Pervious surface importance drops from June to October to December, to reach less importance than building height in December. This can be explained by seasonal variation of plant cover and soil moisture, the nocturnal temperature difference being reduced between pervious and impervious surfaces during the loss of vegetation and moistening of the soil, as discussed before.

3.7.3. Inter-group normalized LST variability

In June, group1 (LCZ 1 and LCZ 2) has the highest temperature. These two classes, consisting of dense areas with small size buildings, mostly paved, differ mainly in their average building height (32 m vs 26 m) (Table 5). It seems that at this height, the vertical dimension doesn't impact the temperature too much. This could be explained by the narrow streets (a mean width of 7 m), with high buildings (> 25 m) which create deep canyons (height-to-width ratio > 3.5) for both classes. Mean temperature drops by 0.4 degrees between Group 1 and Group 2. The latter includes densely built areas with small size buildings, mostly paved, with low building height (LCZ 3) and moderately dense zones, with moderate pervious land cover fraction, medium size but high buildings (LCZ 4). Unlike group 1, the big difference of building height between these two classes has a significant impact on temperature. Group 3 shows a further decrease in temperature (difference of 0.5 degrees between group 2 and group 3). Group 3 includes open mid-rise zones, with medium size buildings and moderate pervious land cover fraction (LCZ 5), large mid-rise blocks in moderately dense areas and mostly paved (LCZ 8), the port area (LCZ 10) and featureless landscape of rock (LCZ E). The presence of vegetation in LCZ 5 has a cooling effect and compensates for the increase in temperature due to size of buildings, resulting in temperature close to areas with large structures on mostly impervious surfaces. There is a net decrease in temperature in group 4 (difference of 0.9 degrees with group 3) when jumping to LCZ classes with high pervious surface fraction of 48% and 70% for abundant vegetation classes (LCZ 6, LCZ 9) and sandy coastal areas (LCZ F) respectively. Finally, there is a difference of 0.5 degrees between group 4 and group 5, where group 5 is made up of the pine forest (LCZ B) and the hippodrome (LCZ C) with a pervious surface fraction $> 70\%$.

In October, LCZ 1 and LCZ 2 are no more significantly different than LCZ 3 and LCZ 4 ending with group 1. LCZ 6, LCZ 9 and LCZ F are no more significantly different than LCZ B and LCZ C ending with group 3. Furthermore, LCZ 10 and LCZ E, mostly impervious surfaces, are closer in temperature to group 3 rather than to group 2 (LCZ 5 and LCZ 8). This could be explained, as previously discussed, by the increase in night LST of pervious wet soil, further reducing the LST difference between the predominantly pervious and impervious LCZs. Group 1, with a mean temperature of 25.4 degrees shows a difference of 0.3 and 0.7 degrees with group 2 and group 3 respectively.

In December in cold weather the compact high-mid-low-rise and open high-rise groups show 0.3 degrees difference with the group consisting of open mid-low-rise and sparsely built zones.

All these results are in-line with the findings of Stewart et al. (2014) (Stewart et al., 2014) "that thermal contrasts exist among LCZ classes, and that such contrasts are governed largely by building height and spacing, pervious surface fraction, tree density, and soil wetness. These contrasts are largest at night, over dry surfaces, and in calm, clear weather. Nocturnal temperatures observed in compact built zones tend to be highest, followed by open and sparsely built zones, and lastly by treed and low plant zones."

3.7.4. Limitations of the study

This study was based on an LCZ map dating from July 2016. It was assumed that no change in urban structure occurred between October 2015, and July 2016. The RF model did not capture temporal variation of LST-LCZ relationship and was rerun for each date. A more generic model would have been useful but would have led to too much complexity. The residual error between the target LST

Table 5

Urban predictors average values: ¹ Ratio of building plan area to total plan area (%), ² Ratio of pervious plan area to total plan area (%), ³ Geometric average of building heights (m), ⁴ Average of building area (m^2); Groups on June 7, October 11 and December 7: ⁵ Average LST of group ($^{\circ}$ C), ⁶ Difference in average LST between two consecutive groups ($^{\circ}$ C).

	Building surface fraction ¹ (%)	Pervious surface fraction ² (%)	Building Height ³ (m)	Building area ⁴ (m^2)	7-Jun-16	11-Oct-15	7-Dec-15
LCZ 1	37	11	32	367	Group 1 (26.3 $^{\circ}$ C) ⁵	(0.4 $^{\circ}$ C) ⁶	Group 1 (12.8 $^{\circ}$ C)
LCZ 2	35	15	26	431			
LCZ 3	40	9	13	200	Group 2 (25.9 $^{\circ}$ C)	(0.5 $^{\circ}$ C)	(0.3 $^{\circ}$ C)
LCZ 4	27	23	36	525			
LCZ 5	21	33	26	569	Group 3 (25.4 $^{\circ}$ C)	(0.4 $^{\circ}$ C)	Group 2 (12.5 $^{\circ}$ C)
LCZ 8	16	14	21	1961			
LCZ 10	15	10	15	3675			
LCZ E	7	11	20	1665	(0.9 $^{\circ}$ C)	Group 3 (24.7 $^{\circ}$ C)	Group 2 (12.5 $^{\circ}$ C)
LCZ 6	16	48	14	977			
LCZ 9	6	48	20	928	Group 4 (24.5 $^{\circ}$ C)	(0.5 $^{\circ}$ C)	Group 2 (12.5 $^{\circ}$ C)
LCZ F	2	70	31	473			
LCZ B	3	85	27	445	Group 5 (24.0 $^{\circ}$ C)	(0.3 $^{\circ}$ C)	Group 1 (12.8 $^{\circ}$ C)
LCZ C	5	71	20	543			

Building surface fraction	Pervious surface fraction		Building height	Building area	
Compact	>= 35	Mostly paved	<= 15	High-rise	> 30
Open	15 - 30	Moderate (low plants)	20 - 35	Mid-rise	15 - 30
Sparsely built	< 10	Abundant (low plants)	48	Low-rise	< 15
		Sand cover	70		
		Scattered trees	> 70		

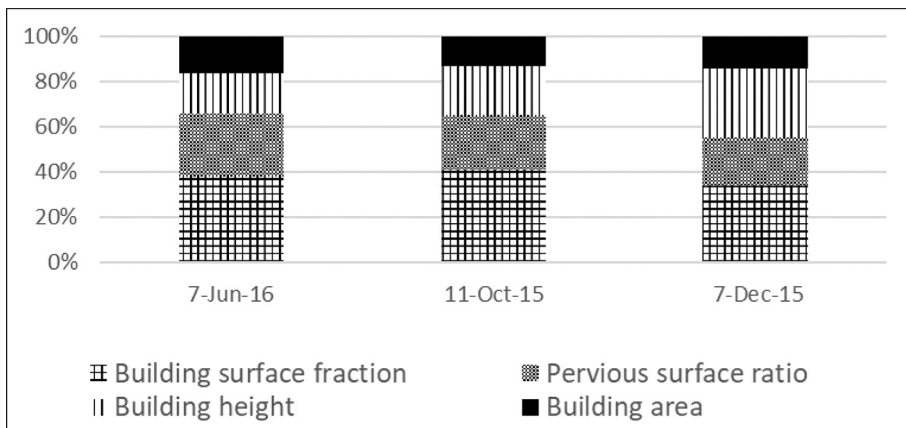


Fig. 8. Importance of urban predictors as calculated by Random Forest model for June 7, 2016; October 11, 2015 and December 7, 2015.

values and the predicted values was attributed solely to the urban structure. A part is probably attributed to topography. LST topographic normalization process could be improved.

4. Conclusion

This study focused on the relationship between topographically normalized LST and LCZ to assess the impact of urban development on land surface temperature in Beirut, a city with a complex topography and a heterogeneous urban morphology. The methodology that was developed for this purpose consisted of three steps: (1) isolate urban influences by topographic normalization using Random Forest regression; (2) perform grouping of LCZs whose temperatures were not significantly different following an ANOVA approach; and (3) express UHII as pairwise difference between mean temperature of the resulting LCZ groups. It was tested at three different dates, under clear and calm weather conditions, favorable to the appearance of UHI. The date chosen accounted for changes in synoptic weather, daily irradiation, and land cover properties (vegetation fraction, soil moisture) during the year. It appeared that UHI was strongest (larger spread of data) and that thermal behavior between different LCZ classes was more differentiated in dry season and hot weather than in wet season and cold weather. The stronger the UHI, the greater the impact of the buildings 3D geometry and surface land cover characteristics on temperature. The main urban variables which contribute to the spatial variability of topographically normalized LST are, in decreasing order of relative importance, the built-up ratio, the pervious surface ratio, the buildings' mean height and mean surface area. The spatial structure of normalized LST followed that of the LCZ for the three selected episodes, although the LCZ units, i.e. contiguous areas of same LCZ type, have on average a diameter of less than 400 m, the minimum value recommended by [Stewart and Oke \(2012\)](#). The results were consistent with other studies indicating that this methodology could be applied to other cities with complex topography. Using a standard methodology allows comparison between cities, which is one of the goals of the LCZ classification.

Intra-urban heat-health-risk maps are usually created by linking population census data (vulnerability index map) to real LST data (hazard index map). [Buscail et al. \(2012\)](#) recommend to “use the risk index together with hazard and vulnerability indices to identify which dimension contributes the most to health risk for a given area” in order to implement the most efficient preventive actions. This study showed the existence of a relationship between topographically normalized LST and LCZ in Beirut. The LCZ map could be considered as a heat-hazard index map due to urban development and would allow to determine where and how to implement mitigation actions, since anthropogenic factors are the only ones which can be acted upon. Mitigation actions cannot be solely based on UHII data ([Martilli et al., 2020](#)). A lower temperature at a certain point does not necessarily mean better thermal comfort ([van Hove et al., 2015](#)). An indicator of thermal comfort, the Physiologically Equivalent Temperature (PET) is controlled by other meteorological parameters than temperature such as air humidity and wind velocity ([Matzarakis and Amelung, 2008](#)) which could be affected by the complex topography of Beirut as well. It would be interesting to build in a second step a heat-health-risk map by combining the LCZ map, a heat-hazard index map due to topography effect, a PET map and demographic data, a map which will be a very useful decision-making tool for heat mitigation measures adapted to the context of each city.

Disaggregating LST into natural and anthropogenic factors, allows to identify which of the two factors contribute the most to intra-urban UHII and how. Consequently, it is recommended to separate the influence of urban structure from that of topography in the study of urban climate to inform the appropriate mitigation actions.

Declaration of Competing Interest

None.

Acknowledgments

We thank the Lebanese National Council for Scientific Research and the research council of the Saint Joseph University for financing the research project on Urban Heat Island in Beirut.

References

- Adjizian-Gérard, J., Zaarour, R., Badaro-Saliba, N., Traboulsi, M., Gérard, P.-C., Bakhache, C., Kehdy, N., El Ess, F., 2013. Beirut faced with climatic aridification. *Sécheresse* 24 (3), 214–223.
- Alexander, P.J., Mills, G., 2014. Local climate classification and Dublin's Urban Heat Island. *Atmosphere* 5 (4), 755–774.
- Alexander, P.J., Mills, G., Fealy, R., 2015. Using LCZ data to run an urban energy balance model. *Urban Clim.* 13, 14–37.
- Alexander, P.J., Fealy, R., Mills, G.M., 2016. Simulating the impact of urban development pathways on the local climate: A scenario-based analysis in the greater Dublin region, Ireland. *Landscape Urban Plan.* 152, 72–89.
- Arnfield, A.J., 2003. Two decades of urban climate research: a review of turbulence, exchanges of energy and water, and the urban heat island. *Int. J. Climatol.* 23 (1), 1–26.
- AST.08.003, 2001. NASA/METI/AIST/Japan Spaceystems, and U.S./Japan ASTER Science Team. ASTER Level 2 Surface Temperature Product. https://doi.org/10.5067/ASTER/AST_08.003. Distributed by NASA EOSDIS Land Processes DAAC. Accessed 2019-06-25.
- ASTER, 2021. User Handbook. https://lpdaac.usgs.gov/documents/262/ASTER_User_Handbook_v2.pdf.
- ASTER GDEM, 2001. NASA/METI/AIST/Japan Spaceystems, and U.S./Japan ASTER Science Team. ASTER DEM Product. <https://doi.org/10.5067/ASTER/AST14DEM.003> distributed by NASA EOSDIS Land Processes DAAC. Accessed 2019-06-25.
- Bartkowiak, P., Castelli, M., Notarnicola, C., 2019. Downscaling land surface temperature from MODIS dataset with random Forest approach over alpine vegetated areas. *Remote Sens.* 11, 1319.
- Bechtel, B., Zásek, K., Hoshyaripour, G., 2012. Downscaling land surface temperature in an urban area: a case study for Hamburg, Germany. *Remote Sens.* 4, 3184–3200.

- Bechtel, B., Alexander, P.J., Böhner, J., Ching, J., Conrad, O., Feddema, J., Mills, G., See, L., Stewart, I., 2015. Mapping local climate zones for a worldwide database of the form and function of cities. *ISPRS Int. J. Geo Inf.* 4 (1), 199–219.
- Bechtel, B., Pesaresi, M., See, L., Mills, G., Ching, J., Alexander, P., Feddema, J., Florczyk, A., Stewart, I., 2016. Towards consistent mapping of urban structures – Global human settlement layer and local climate zones. In: *ISPRS - International Archives of the Photogrammetry, Remote Sensing and Spatial Information Sciences* XLI-B8, pp. 1371–1378.
- Bechtel, B., Demuzere, M., Mills, G., Zhan, W., Sismanidis, P., Small, C., Voogt, J., 2019. SUHI analysis using local climate zones—A comparison of 50 cities. *Urban Clim.* 28, 100451.
- Bernard, J., Bocher, E., Petit, G., Palominos, S., 2018. Sky view factor calculation in Urban context: computational performance and accuracy analysis of two open and free GIS tools. *Climate* 6 (3), 60.
- Bokwa, A., Hajto, M., Walawender, J., Szumanowski, M., 2015. Influence of diversified relief on the urban heat island in the city of Krakw, Poland. *Theor. Appl. Climatol.* 122.
- Bradter, U., Kunin, W.E., Altringham, J.D., Thom, T.J., Benton, T.G., 2013. Identifying appropriate spatial scales of predictors in species distribution models with the random forest algorithm. *Methods Ecol. Evol.* 4 (2), 167–174.
- Breiman, L., 2001. Random forests. *Mach. Learn.* 45 (1), 5–32.
- Brousse, O., Martilli, A., Foley, M., Mills, G., Bechtel, B., 2016. WUDAPT, an efficient land use producing data tool for mesoscale models? Integration of urban LCZ in WRF over Madrid. *Urban Clim.* 17, 116–134.
- Buscail, C., Upegui, E., Viel, J.-F., 2012. Mapping heatwave health risk at the community level for public health action. *Int. J. Health Geogr.* 11 (1), 38.
- Cai, M., Ren, C., Xu, Y., 2017a. Investigating the relationship between local climate zone and land surface temperature. In: 2017 Joint Urban Remote Sensing Event (JURSE). IEEE, Dubai, United Arab Emirates, pp. 1–4. <http://ieeexplore.ieee.org/document/7924622/> (Last accessed 21 June 2020).
- Cai, M., Ren, C., Xu, Y., Lau, K., Wang, R., 2017b. Investigating the relationship between local climate zone and land surface temperature using an improved WUDAPT methodology – A case study of Yangtze River Delta, China. *Urban Clim.* 24.
- Catani, F., Lagomarsino, D., Segoni, S., Tofani, V., 2013. Landslide susceptibility estimation by random forests technique: sensitivity and scaling issues. *Nat. Hazards Earth Syst. Sci.* 13, 2815–2831.
- Central Administration of Statistics - Population, 2021. <http://www.cas.gov.lb/index.php/demographic-and-social-en/population-en> (Last accessed 21 June 2020).
- Chelala, C., Gerard, J., Abboud, M., Farah, W., Rizk, T., 2006. Transport routier et pollution de l'air dans Beyrouth Municipale (Liban).
- Chelala, C., Maignant, G., Zaarour, R., Saliba, N., Abboud, M., Farah, W., 2007. Transports urbains et pollution de l'air à Beyrouth-Municipale (Liban): Application du modèle STREET.
- Chen, Q., Ding, M., Yang, X., Hu, K., Qi, J., 2018. Spatially explicit assessment of heat health risk by using multi-sensor remote sensing images and socioeconomic data in Yangtze River Delta, China. *Int. J. Health Geogr.* 17 (1), 15.
- Cutler, A., Cutler, D.R., Stevens, J.R., 2012. Random forests. In: Zhang, C., Ma, Y. (Eds.), *Ensemble Machine Learning: Methods and Applications*. Springer US, Boston, MA, pp. 157–175. https://doi.org/10.1007/978-1-4419-9326-7_5 (Last accessed 19 February 2021).
- da Silva, V.J., da Silva, C.R., da Silva Almeida, L., Silva, C., de Paula Carvalho, H., de Camargo, R., 2018. Mobile transect for identification of intra-urban heat islands in Uberlandia, Brazil. *Revista Ambiente Água* 13 (4). http://www.scielo.br/scielo.php?script=sci_abstract&pid=S1980-993X2018000400303&lng=en&nrm=iso&tlang=en (Last accessed 20 June 2020).
- Das, M., Das, A., Mandal, S., 2020. Outdoor thermal comfort in different settings of a tropical planning region: A study on Sriniketan-Santiniketan planning area (SSPA), eastern India. *Sustain. Cities Soc.* 63, 102433.
- Davenport, A., Grimm, C., Oke, T., Wieringa, J., 2000. Estimating the roughness of cities and sheltered country. In: 15th Conference on Probability and Statistics in the Atmospheric Sciences/12th Conference on Applied Climatology. American Meteorological Society, Asheville, NC, pp. 96–99.
- Deilami, K., Kamruzzaman, Md., Liu, Y., 2018. Urban heat island effect: A systematic review of spatio-temporal factors, data, methods, and mitigation measures. *Int. J. Appl. Earth Obs. Geoinf.* 67, 30–42.
- Del Pozo, S., Landes, T., Nerry, F., Kastendech, P., Najjar, G., Philippis, N., Laguela, S., 2020. UHI estimation based on ASTER and MODIS satellite imagery: first results on Strasbourg city, France. In: Conférence ISPRS XXIV, p. 8. <http://icube-publis.unistra.fr/4-DLNK20>.
- Dian, C., Pongrácz, R., Dezső, Z., Bartholy, J., 2020. Annual and monthly analysis of surface urban heat island intensity with respect to the local climate zones in Budapest. *Urban Clim.* 31, 100573.
- Doan, T., Kalita, J., 2015. Selecting machine learning algorithms using regression models. In: 2015 IEEE International Conference on Data Mining Workshop (ICDMW). IEEE, Atlantic City, NJ, USA, pp. 1498–1505. <http://ieeexplore.ieee.org/document/7395848/> (Last accessed 18 February 2021).
- EarthExplorer, 2021. <https://earthexplorer.usgs.gov/> (Last accessed 20 November 2020).
- Fenner, D., Meier, F., Bechtel, B., Otto, M., Scherer, D., 2017. Intra and inter 'local climate zone' variability of air temperature as observed by crowdsourced citizen weather stations in Berlin, Germany. *Meteorol. Z.* 525–547.
- Florinsky, I., Kuryakova, G., 2000. Determination of grid size for digital terrain modeling in landscape investigations - exemplified by soil moisture distribution at a micro-scale. *Int. J. Geogr. Inf. Sci.* 14, 815–832.
- Founda, D., Santamouris, M., 2017. Synergies between Urban Heat Island and heat waves in Athens (Greece), during an extremely hot summer (2012). *Sci. Rep.* 7.
- Fox, E.W., Hill, R.A., Leibowitz, S.G., Olsen, A.R., Thornbrugh, D.J., Weber, M.H., 2017. Assessing the accuracy and stability of variable selection methods for random forest modeling in ecology. *Environ. Monit. Assess.* 189 (7), 316.
- Gabriel, K.M.A., 2011. Urban and rural mortality rates during heat waves in Berlin and Brandenburg, Germany. *Environ. Pollut.* 7.
- Geiger, R., Aron, R.H., Todhunter, P., 2003. *The Climate near the Ground*. Rowman & Littlefield.
- Geletić, J., Lehner, M., 2016. GIS-based delineation of local climate zones: the case of medium-sized central European cities. *Moravian Geogr. Rep.* 24, 2–12.
- Geletić, J., Lehner, M., Dobrovolny, P., 2016. Land surface temperature differences within local climate zones, based on two central European cities. *Remote Sens.* 8, 788.
- Genuer, R., Poggio, J.-M., Tuleau-Malot, C., 2010. Variable selection using random forests. *Pattern Recogn. Lett.* 31 (14), 2225–2236.
- Geopedia - Wudapt, 2021. https://geopedia.world/#T4_x241526.67743835386_y5061411.592702443_s15_b2345 (Last accessed 20 November 2020).
- Gercek, D., Güven, I., Oktay, I., 2016. Analysis of the intra-city variation of urban heat island and its relation to land surface/cover parameters. In: *ISPRS Annals of Photogrammetry, Remote Sensing and Spatial Information Sciences* III–8, pp. 123–129.
- Ghadban, M., Baayoun, A., Lakxis, I., Najem, S., Saliba, N.A., Shihadeh, A., 2020. A novel method to improve temperature forecast in data-scarce urban environments with application to the Urban Heat Island in Beirut. *Urban Clim.* 33, 100648.
- Gholami, R., Beck, C., 2019. Towards the determination of driving factors of varying LST-LCZ relationships: a case study over 25 cities. *Geogr. Pannonica* 23, 289–307.
- Goggins, W.B., Chan, E.Y.Y., Ng, E., Ren, C., Chen, L., 2012. Effect modification of the association between short-term meteorological factors and mortality by Urban Heat Islands in Hong Kong. *PLoS One* 7 (6), e38551.
- Gray, T.N.E., Phan, C., Long, B., 2010. Modelling species distribution at multiple spatial scales: gibbon habitat preferences in a fragmented landscape: gibbon distribution in fragmented landscapes. *Anim. Conserv.* 13 (3), 324–332.
- Grohmann, C., 2015. Effects of spatial resolution on slope and aspect derivation for regional-scale analysis. *Comput. Geosci.* 77.
- Hais, M., Kucera, T., 2009. The influence of topography on the forest surface temperature retrieved from Landsat TM, ETM + and ASTER thermal channels. *ISPRS J. Photogramm. Remote Sens.* 64, 585–591.
- Hastie, T., Tibshirani, R., Friedman, J., 2009. Random forests. In: Hastie, T., Tibshirani, R., Friedman, J. (Eds.), *The Elements of Statistical Learning: Data Mining, Inference, and Prediction*, Springer Series in Statistics. Springer, New York, NY, pp. 587–604. https://doi.org/10.1007/978-0-387-84858-7_15 (Last accessed 20 February 2021).
- He, J., Zhao, W., Li, A., Wen, F., Yu, D., 2018. The impact of the terrain effect on land surface temperature variation based on Landsat-8 observations in mountainous areas. *Int. J. Remote Sens.* 40, 1–20.

- Heaviside, C., Vardoulakis, S., Cai, X.-M., 2016. Attribution of mortality to the urban heat island during heatwaves in the west midlands, UK. *Environ. Health* 15 (1), S27.
- HEG-C, 2017. HDF-EOS to GeoTIFF Converter (HEG-C). Earth Science Data and Information System (ESDIS) Project, Earth Science Projects Division (ESPD), Flight Projects Directorate, Goddard Space Flight Center (GSFC) National Aeronautics and Space Administration (NASA). URL (EOSDIS Tools and Services Portfolio Entry), Greenbelt, MD v2.14. <https://bugs.earthdata.nasa.gov/browse/ETSP-260?src=confmacro>.
- Hidalgo, J., Dumas, G., Masson, V., Petit, G., Bechtel, B., Bocher, E., Foley, M., Schoetter, R., Mills, G., 2019. Comparison between local climate zones maps derived from administrative datasets and satellite observations. *Urban Clim.* 27, 64–89.
- Hu, Y., Hou, M., Jia, G., Zhao, C., Chen, X., Yu, Y., 2019. Comparison of surface and canopy urban heat islands within megacities of eastern China. *ISPRS J. Photogramm. Remote Sens.* 156, 160–168.
- Hutengs, C., Vohland, M., 2016. Downscaling land surface temperatures at regional scales with random forest regression. *Remote Sens. Environ.* 178, 127–141.
- Imamura, I.R., 1970. Role of soil moisture in the determination of urban heat island intensity in different climate regimes. *WIT Trans. Ecol. Environ.* 1, 395–402.
- Johnson, D., Lulla, V., Stanforth, A., Webber, J., 2011. Remote sensing of heat-related health risks: the trend toward coupling socioeconomic and remotely sensed data: remote sensing of heat-related health risks. *Geogr. Compass* 5 (10), 767–780.
- Kaloustian, N., Bechtel, B., 2016. Local climatic zoning and urban heat island in Beirut. *Procedia Eng.* 169, 216–223.
- Laaidi, K., Zeghnoun, A., Douset, B., Bretin, P., Vandendorren, S., Giraudet, E., Beaudeau, P., 2012. The impact of heat Islands on mortality in Paris during the august 2003 heat wave. *Environ. Health Perspect.* 120 (2), 254–259.
- Lagomarsino, D., Tofani, V., Segoni, S., Catani, F., Casagli, N., 2017. A tool for classification and regression using random forest methodology: applications to landslide susceptibility mapping and soil thickness modeling. *Environ. Model. Assess.* 22.
- Lau, K., Ren, C., Shi, Y., Zheng, V., Yim, S.H.L., Lai, M., 2015. Determining the Optimal Size of Local Climate Zones for Spatial Mapping in High-Density Cities.
- Li, Z.-L., Si, M., Leng, P., 2020. A review of remotely sensed surface Urban Heat Islands from the fresh perspective of comparisons among different regions (invited review). *Prog. Electromagn. Res.* 102, 31–46.
- Lindberg, F., Grimmond, C., Gabey, A., Huang, B., Kent, C., Sun, T., Theeuwes, N., Järvi, L., Ward, H., Capel-Timms, I., Chang, Y., Jonsson, P., Krave, N., Liu, D., Meyer, D., Olofson, F., Tan, J., Wästberg, D., Xue, L., Zhang, Z., 2018. Urban multi-scale environmental predictor (UMEP): an integrated tool for city-based climate services. *Environ. Model. Softw.* 99, 70–87.
- Lookingbill, T.R., Urban, D.L., 2003. Spatial estimation of air temperature differences for landscape-scale studies in montane environments. *Agricul. Forest Meteorol.* 11.
- Lotfian, M., Ingensand, J., Composto, S., Molinari, M., Brovelli, M., 2019. The Relationship between Land Surface Temperature and Local Climate Zone Classification: A Case Study of the Canton Geneva, Switzerland.
- Malbeteau, Y., Merlin, O., Gascoin, S., Gastellu-Etchegorry, J.-P., Mattar, C., Olivera-Guerra, L., Khabba, S., Jarlan, L., 2017. Correcting land surface temperature data for elevation and illumination effects in mountainous areas: a case study using ASTER data over a steep-sided valley in Morocco. *Remote Sens. Environ.* 189, 25–39.
- Manandhar, P., Bande, L., Tsoupos, A., Marpu, P., Armstrong, P., 2019. A study of local climate zones in Abu Dhabi with urban weather stations and numerical simulations. *Sustainability* 12, 156.
- Manoli, G., Faticchi, S., Schläpfer, M., Yu, K., Crowther, T.W., Meili, N., Burlando, P., Katul, G.G., Bou-Zeid, E., 2019. Magnitude of urban heat islands largely explained by climate and population. *Nature* 573 (7772), 55–60.
- Manoli, G., Faticchi, S., Bou-Zeid, E., Katul, G.G., 2020. Seasonal hysteresis of surface urban heat islands. *Proc. Natl. Acad. Sci.* 117 (13), 7082–7089.
- Martilli, A., Krayenhoff, E.S., Nazarian, N., 2020. Is the Urban Heat Island intensity relevant for heat mitigation studies? *Urban Clim.* 31, 100541.
- Matzarakis, A., Amelung, B., 2008. Physiological equivalent temperature as Indicator for impacts of climate change on thermal comfort of humans. In: Thomson, M.C., García-Herrera, R., Beniston, M. (Eds.), *Seasonal Forecasts, Climatic Change and Human Health*. Springer Netherlands, Dordrecht, pp. 161–172. https://doi.org/10.1007/978-1-4020-6877-5_10 (Last accessed 8 December 2020).
- McCune, B., 2007. Improved estimates of incident radiation and heat load using non-parametric regression against topographic variables. *J. Veg. Sci.* 18, 751–754.
- Mughal, D.M., Li, X.-X., Yin, T., Martilli, A., Brousse, O., Dissegna, A., Norford, L., 2019. High-resolution, multi-layer modelling of Singapore's urban climate incorporating local climate zones. *J. Geophys. Res. Atmos.* 124 <https://doi.org/10.1029/2018JD029796>.
- Oke, T., 1982. The energetic basis of urban heat island. *Q. J. R. Meteorol. Soc.* 108, 1–24.
- Oke, T., 1988. The urban energy balance. *Prog Phys Geogr. Prog. Phys.* 12, 471–508.
- Pang, B., Yue, J., Zhao, G., Xu, Z., 2017. Statistical downscaling of temperature with the random forest model. In: Gonzalez, J.E. (Ed.), *Advances in Meteorology* 2017, 7265178.
- Pierce, K., Lookingbill, T., Urban, D., 2005. A simple method for estimating potential relative radiation (PRR) for landscape-scale vegetation analysis. *Landsc. Ecol.* 20, 137–147.
- Quan, J., 2019. Multi-temporal effects of Urban forms and functions on Urban Heat Islands based on local climate zone classification. *Int. J. Environ. Res. Public Health* 16 (12). <https://europepmc.org/article/PMC/6617371> (Last accessed 21 June 2020).
- Richard, Y., Emery, J., Dudek, J., Pergaud, J., Chateau-Smith, C., Zito, S., Rega, M., Vairet, T., Castel, T., Thevenin, T., Pohl, B., 2018. How relevant are local climate zones and Urban climate zones for urban climate research? Dijon (France) as a case study. *Urban Clim.* 26, 258–274.
- Ruel, J.-C., Pin, D., Cooper, A., 1998. Effect of topography on wind behaviour in a complex terrain. *Forestry* 71.
- Saliba, Nada, Gerard, J., Zaarour, R., Abboud, M., Farah, W., Saliba, Najat, Shihadeh, A., 2013. A geostatistical approach for assessing population exposure to NO 2 in a complex urban area (Beirut, Lebanon). *Stoch. Env. Res. Risk A.* 28, 467–474.
- Santamouris, M., 2015. Analyzing the heat island magnitude and characteristics in one hundred Asian and Australian cities and regions. *Sci. Total Environ.* 512–513, 582–598.
- Shi, Y., Xiang, Y., Zhang, Y., 2019. Urban Design factors influencing surface urban heat island in the high-density city of Guangzhou based on the local climate zone. *Sensors (Basel, Switzerland)* 19, 16. <https://www.ncbi.nlm.nih.gov/pmc/articles/PMC6721248/> (Last accessed 21 June 2020).
- Smargiassi, A., Goldberg, M.S., Plante, C., Fournier, M., Baudouin, Y., Kosatsky, T., 2009. Variation of daily warm season mortality as a function of micro-urban heat islands. *J. Epidemiol. Community Health* 63 (8), 659–664.
- Spacesystems, N., 2001. ASTER Level 2 Surface Temperature Product. https://lpdaac.usgs.gov/products/ast_08v003/.
- Stewart, I., Oke, T., 2009. Newly Developed "Thermal Climate Zones" for Defining and Measuring Urban Heat Island "Magnitude" in the Canopy Layer.
- Stewart, I.D., Oke, T.R., 2012. Local climate zones for Urban temperature studies. *Bull. Am. Meteorol. Soc.* 93 (12), 1879–1900.
- Stewart, I.D., Oke, T.R., Krayenhoff, E.S., 2014. Evaluation of the 'local climate zone' scheme using temperature observations and model simulations. *Int. J. Climatol.* 34 (4), 1062–1080.
- Stroppiana, D., Antoninetti, M., Brivio, P., 2014. Seasonality of MODIS LST over southern Italy and correlation with land cover, topography and solar radiation. *Eur. J. Remote Sens.* 47, 133–152.
- Tan, J., Zheng, Y., Tang, X., Guo, C., Li, L., Song, G., Zhen, X., Yuan, D., Kalkstein, A., Li, F., 2009. The urban heat island and its impact on heat waves and human health in Shanghai. *Int. J. Biometeorol.* 54, 75–84.
- Tomlinson, C.J., Chapman, L., Thornes, J.E., Baker, C.J., 2011. Including the urban heat island in spatial heat health risk assessment strategies: a case study for Birmingham, UK. *Int. J. Health Geogr.* 10 (1), 42.
- Tzavalis, A., Paravantis, J., Mihalakakou, G., Fotiadi, A., Stigka, E., 2015. Urban heat island intensity: a literature review. *Fresenius Environ. Bull.* 24, 4537–4554.
- US EPA, O, 2014a. Heat Island Compendium. US EPA. <https://www.epa.gov/heatislands/heat-island-compendium> (Last accessed 14 December 2020).
- US EPA, O, 2014b. Heat Island Impacts. US EPA. <https://www.epa.gov/heatislands/heat-island-impacts> (Last accessed 28 November 2020).
- US EPA, O, 2014c. Learn about Heat Islands. US EPA. <https://www.epa.gov/heatislands/learn-about-heat-islands> (Last accessed 21 June 2020).
- van Hove, L.W.A., Jacobs, C.M.J., Heusinkveld, B.G., Elbers, J.A., van Driel, B.L., Holtslag, A.A.M., 2015. Temporal and spatial variability of urban heat island and thermal comfort within the Rotterdam agglomeration. *Build. Environ.* 83, 91–103.

- Verdonck, M.-L., Okujeni, A., van der Linden, S., Demuzere, M., Dewulf, R., Vancoillie, F., 2017. Influence of neighbourhood information on "local climate zone" mapping in heterogeneous cities. *Int. J. Appl. Earth Obs. Geoinf.* 62, 102–113.
- Voogt, J.A., Oke, T.R., 2003. Thermal remote sensing of urban climates. *Remote Sens. Environ.* 86 (3), 370–384.
- Wang, C., Middel, A., Myint, S., Kaplan, S., Brazel, A., Lukasczyk, J., 2018. Assessing local climate zones in arid cities: the case of Phoenix, Arizona and Las Vegas, Nevada. *ISPRS J. Photogramm. Remote Sens.* 141.
- Weng, Q., Lu, D., Schubring, J., 2004. Estimation of land surface temperature–vegetation abundance relationship for urban heat island studies. *Remote Sens. Environ.* 89 (4), 467–483.
- Wicki, A., Parlow, E., 2017. Attribution of local climate zones using a multitemporal land use/land cover classification scheme. *J. Appl. Remote. Sens.* 11.
- Wicki, A., Parlow, E., Feigenwinter, C., 2018. Evaluation and modeling of Urban Heat Island intensity in Basel, Switzerland. *Climate* 6.
- Xilin, Z., Okaze, T., Ren, C., Cai, M., Ishida, Y., Mochida, A., 2020. Mapping local climate zones for a Japanese large city by an extended workflow of WUDAPT level 0 method. *Urban Clim.* 33, 100660.
- Xu, Y., Ren, C., Ma, P., Ho, J., WANG, W., Lau, K., Lin, H., Ng, E., 2017. Urban morphology detection and computation for urban climate research. *Landsc. Urban Plan.* 167, 212–224.
- Xue, J., You, R., Liu, W., Chen, C., Lai, D., 2020. Applications of local climate zone classification scheme to improve Urban sustainability: A bibliometric review. *Sustainability* 12 (19), 8083.
- Yan, H., Fan, S., Guo, C., Hu, J., Dong, L., 2014. Quantifying the impact of land cover composition on intra-Urban air temperature variations at a mid-Latitude City. *PLoS One* 9 (7), e102124.
- Yang, J., Zhan, Y., Xiao, X., Xia, J.C., Sun, W., Li, X., 2020. Investigating the diversity of land surface temperature characteristics in different scale cities based on local climate zones. *Urban Clim.* 34, 100700.
- Yu, Z., Xu, S., Zhang, Y., Jorgensen, G., Vejre, H., 2018. Strong contributions of local background climate to the cooling effect of urban green vegetation. *Sci. Rep.* 8.
- Zaarour, R., Voiron-Canicio, C., 2020. Les transformations morphologiques du tissu bâti de Beyrouth depuis 1950. Analyse morpho-dynamique à échelle fine. Méditerranée. Revue géographique des pays méditerranéens. *J. Mediterranean Geogr.* 131. <http://journals.openedition.org/mediterranee/11208> (Last accessed 5 July 2020).
- Zaarour, R., Voiron-Canicio, C., Buccianti-Barakat, L., 2008. Crédit de données dans un contexte imprécis et incertain: application à la dynamique urbaine de Beyrouth (1956-1999), pp. 141–150.
- Zaarour, R., Gerard, J., Saliba, N., Harb, J., Gerard, P.-C., 2015. La variabilité spatiale de l'indice de vulnérabilité urbaine face à l'aléa sismique: Le cas de Beyrouth. Actes du colloque Risque sismique: aléas, vulnérabilités et incertitudes –Liban et pourtour méditerranéen, USJ du 18 au 20 novembre 2014 Volume 36. Beirut.
- Zaarour, R., Saliba, N., Najjar, G., Kupelian, L., Gerard, J., 2021. Fine-scale Mapping of Local Climate Zone for the city of Beirut. Manuscript in preparation.
- Zhao, C., 2018. Linking the local climate zones and land surface temperature to investigate the surface urban heat island, a case study of San Antonio, Texas, U.S.. In: *ISPRS Annals of Photogrammetry, Remote Sensing and Spatial Information Sciences IV-3*, pp. 277–283.
- Zhao, W., Duan, S.-B., Li, A., Yin, G., 2019. A practical method for reducing terrain effect on land surface temperature using random forest regression. *Remote Sens. Environ.* 221, 635–649.
- Zheng, Y., Ren, C., Xu, Y., Wang, R., Ho, J., Lau, K., Ng, E., 2018. GIS-based mapping of local climate zone in the high-density city of Hong Kong. *Urban Clim.* 24, 419–448.
- Zhou, B., Lauwaet, D., Hooyberghs, H., De Ridder, K., Kropp, J.P., Rybski, D., 2016. Assessing seasonality in the surface Urban Heat Island of London. *J. Appl. Meteorol. Climatol.* 55 (3), 493–505.
- Zhou, D., Xiao, J., Bonafoni, S., Berger, C., Deilami, K., Zhou, Y., Frolking, S., Yao, R., Qiao, Z., Sobrino, J., 2018. Satellite remote sensing of surface Urban Heat Islands: Progress, challenges, and perspectives. *Remote Sens.* 11.
- Zhou, X., Okaze, T., Ren, C., Cai, M., Ishida, Y., Watanabe, H., Mochida, A., 2020. Evaluation of urban heat islands using local climate zones and the influence of sea-land breeze. *Sustain. Cities Soc.* 55, 102060.